On Deembedding of Port Discontinuities in Full-Wave CAD Models of Multiport Circuits

Vladimir I. Okhmatovski, *Member, IEEE*, Jason Morsey, *Student Member, IEEE*, and Andreas C. Cangellaris, *Fellow, IEEE*

***Abstract*—A systematic numerical methodology is proposed for the accurate deembedding of multiport discontinuities in full-wave numerical models of multiconductor microwave and millimeter-wave passive structures and high-speed digital interconnects. The discussed methodology is based on the earlier-proposed short-open calibration (SOC) procedure. The latter being a numerical analog of the experimental transmission-thru-reflection technique provides a consistent removal of the feed networks of the device-under-test over a wide range of frequencies. The treatment of multiport topologies is achieved through the continuation of the original scalar SOC method into the vector space. The new vector SOC method is easily combined with integral-equation-based method-of-moments electromagnetic-field solvers and allows for substantial flexibility in the choice of excitation mechanisms. Such commonly used method-of-moments driving schemes as ports locally backed up by a vertical conducting wall, ungrounded-internal differential ports, and via-mounted ports can be accurately deembedded within the framework of the vector SOC. Several numerical experiments are provided to validate the proposed multiport deembedding methodology and demonstrate its application.**

***Index Terms*—Deembedding, full-wave computer-aided design (CAD), method of moments (MoM), multiport, short-open calibration (SOC).**

I. Introduction

THE integral-equation (IE)-based method of moments (MoM) has established itself as an accurate and efficient tool for modeling of electromagnetic (EM) propagation, coupling, and radiation phenomena in complex microwave circuits embedded in multilayered planar substrates. Within the framework of time–harmonic fields, both spatial- [1]–[3] and spectral-domain [4], [5] techniques have been successfully implemented. Due to the surface discretization of the circuit instead of the volumetric discretization of the space around it, the IE-based MoM is known to provide higher numerical efficiency [6] compared to the differential-equation methods [7], [8] for the aforementioned class of planar circuit structures. However, unlike the finite-element and finite-difference time-domain methods, allowing for easy application of the principal mode excitation, the IE MoM exhibits a distinct difficulty in the implementation of adequate excitation mechanisms [9], [10]. The complications arise from the fact that while the proper delivery of the principal quasi-TEM mode to the reference planes of the circuit requires the uniform transmission lines to extend to infinity, it is desirable for the numerical implementation of the MoM-based solver that the volume of the modeled circuit remains finite. The most commonly used approaches to circumvent this difficulty are briefly summarized below.

In [10], the traveling-wave excitation was implemented, where the introduction of entire-domain traveling-wave basis functions on the infinite transmission lines allowed for their compact incorporation in the MoM model. Even though this technique preserves the correct physics of the circuit excitation, numerical difficulties associated with the evaluation of the semi-infinite reaction integrals for the transmission-line currents make it rather cumbersome for general-purpose multilayered multiport structure implementation.

An alternative approach, called impressed-field excitation, utilizes the concept of the δ-gap generator and owes its name to the fact that the electric field is impressed at an infinitely small gap between the stub end of the transmission line and the perfect electric conductor (PEC) plane providing the ground reference for the formed voltage generator [9], [11], [12]. Since this excitation mechanism yields a finite-volume structure for MoM discretization, while at the same time providing for an effective launching of the quasi-TEM modes in the transmission lines, the method has been widely adopted. A concern in the implementation of such a model is the presence of the PEC wall used to back the gap generator, which may not be a part of the actual structure. In such cases, in addition to the undesirable presence of spurious contributions from reflections of the surface waves by the PEC walls, a shielded-box Green's function must be employed to account for the introduced PEC walls. To address this issue, a successful attempt has been made recently to utilize the fact that the PEC walls are, in fact, only locally attached to the ports of the circuit [5], [13] and, thus, their influence can be restricted to the feeding transmission lines only. In this way, the unbounded environment around the device is accurately simulated and, at the same time, the conventional δ-gap excitation is enforced.

In [14], the concept of the δ-gap generator was used in alternative excitation schemes such as the internal-ungrounded ports and via-ports where the introduction of the PEC walls is avoided. The deembedding of the port discontinuities can then be accomplished through the standing-wave characterization

Manuscript received April 9, 2003. This work was supported by the Defense Advanced Research Projects Agency under the NeoCAD Program and by the Semiconductor Research Corporation.

V. I. Okhmatovski and A. C. Cangellaris are with the Center for Computational Electromagnetics, Department of Electrical and Computer Engineering, University of Illinois at Urbana-Champaign, Urbana, IL 61801 USA.

J. Morsey was with the Center for Computational Electromagnetics, Department of Electrical and Computer Engineering, University of Illinois at Urbana-Champaign, Urbana, IL 61801 USA. He is now with the IBM T. J. Watson Research Center, Yorktown Heights, NY 10598 USA.

Digital Object Identifier 10.1109/TMTT.2003.820159

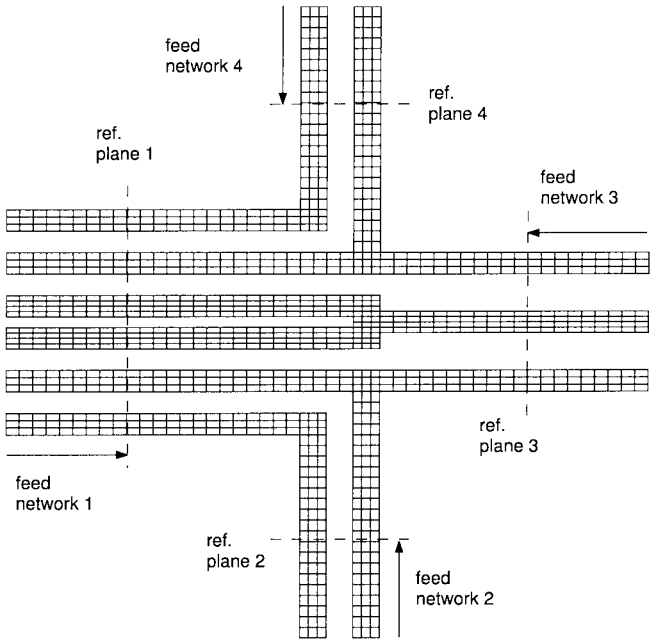

Fig. 1. Geometry of a generic multiport microwave circuit and its MoM discretization.

or through the subtraction of the stub impedances from the differential impedances of the ungrounded ports. In the case of via-ports, it is shown that the differential port connected to the ground plane through the via can be considered directly without any deembedding. However, the methodologies discussed in this paper, other than the standing-wave characterization, result in a rather rough approximation of the network parameters since the higher order fringe fields are not accounted for in the models.

Another methodology, called the matched load simulation (MLS), developed for deembedding of port discontinuities in open printed circuits, was presented in [15]. The MLS enables the use of a finite-size circuit area for the MoM modeling discretization through the simulation of the matched loaded output at the ends of the termination lines. The matching is achieved through the enforcement of the known functional dependence of the traveling-wave current distribution on a relatively short segments of the transmission lines attached to the "quiet" ports. At the same time, the impressed field of the δ-gap generator is moved sufficiently far away from the reference plane of the driven port to allow for the accurate retrieval of the scattering parameters from the standing-wave pattern of the current. Obviously, the implementation of the MLS, similar to all standing-wave characterization schemes for multiport networks, requires computation of the cross-sectional current distribution and the propagation constants of the quasi-TEM eigenmodes of the associated multiconductor transmission-line (MTL) networks [16].

In this paper, a systematic methodology is introduced and demonstrated for broad-band deembedding of the port discontinuities involved in complex multiport microwave systems (Fig. 1). The proposed methodology is based on the concept of short-open calibration (SOC). The idea of SOC was originally proposed for two-port circuits [13]. In [17], the performance of the SOC deembedding was compared with other conventional techniques and was shown to be the most accurate and consistent. It should be pointed out that the SOC method of [13] and [17] was intended for use in conjunction with the aforementioned model of the locally attached δ-gap generators [5]. In this paper, the original "scalar" SOC technique is extended to the vector space. It is aimed at handling structures that involve multiple coupled ports and is referred to as vector short-open calibration (VSOC) method. At the same time, through the numerical examples used for validation of the proposed deembedding methodology, it is shown that it is applicable to most commonly used excitation mechanisms in the MoM modeling of planar circuits. More specifically, the excitation schemes of a locally attached PEC wall backing up the end of the transmission lines, an ungrounded internal port (i.e., open-stub port), and a via-port, can all be easily accommodated. This substantial flexibility in the choice of the excitation mechanisms can be exercised due to the distributed nature of the microwave circuits. Namely, it is understood that any port whether it is referenced to the ground plane or to a local ground represented by the open stub [14] may serve as a launcher of the eigenmodes in the feed interconnect circuits, bringing the signal to the reference planes of the multiport device-under-test (DUT). Therefore, for as long as this particular mechanism effectively excites the quasi-TEM eigenmodes in the planar interconnect feed structure and, subsequently, can be deembedded accurately, thus providing conventional wave port at the reference planes of the DUT, it can be effectively utilized for MoM-based EM modeling. The above discussion makes clear that the presence of PEC walls backing up the δ-gap generator is merely viewed as one of the possible excitation options, but by no means a modeling requirement. Thus, the proposed VSOC technique enables accurate and systematic modeling of multiport unbounded planar circuits while providing significant flexibility in the implementation of the MoM and the choice of excitation models.

This paper is organized as follows. In Section II, the MoM modeling scheme adopted for our purposes is reviewed along with the various excitation mechanisms that can be utilized. In Section III, the VSOC methodology is presented and the transmission matrices for the multiport feed networks are obtained. The deembedding scheme based on the theory of cascaded $\boldsymbol{S}$-matrices is presented in Section IV. The numerical studies of Section V are used to demonstrate the validity of the proposed VSOC methodology and discuss the impact of the commonly used assumption of noninteracting feed networks on the accuracy of deembedding. Finally, Section VI concludes this paper with a brief summary of the method and a few remarks about its attributes.

II. MoM and Excitation Models

The mathematical statement of the EM boundary value problem in terms of surface IEs is usually obtained through the dyadic Green's theorem or the equivalence principle applied to the distinct volumes of the structure under consideration [18]. The most commonly used formulation is the electric-field integral equation (EFIE) in the standard [11] or mixed-potential

[1], [14], [19] forms. Under the assumption of a PEC surface, the EFIE forces the tangential electric field produced by the current $\boldsymbol{J}^e$ flowing on the surface of the conducting portions of the circuit S to cancel the applied tangential electric field $\boldsymbol{E}^{\text{inc}}$ on the same surface S. This is formally expressed as

$$\hat{\boldsymbol{n}} \times \int_S \bar{\bar{\boldsymbol{G}}}(\boldsymbol{r}, \boldsymbol{r}') \cdot \boldsymbol{J}^e(\boldsymbol{r}') d\boldsymbol{r}' = -\hat{\boldsymbol{n}} \times \boldsymbol{E}^{\text{inc}}(\boldsymbol{r}), \qquad \boldsymbol{r} \in S. \tag{1}$$

In (1), $\bar{\bar{\boldsymbol{G}}}$ is the dyadic Green's function of the layered media [20], [21] the circuit is embedded in, $\hat{\boldsymbol{n}}$ is the unit normal vector to S, and $\boldsymbol{r}$ and $\boldsymbol{r}'$ are the position vectors of the observation and source points, respectively. The incident field $\boldsymbol{E}^{\text{inc}}$, uniformly distributed across the width of the conductor, is usually applied at the infinitely narrow gap, thus forming a voltage source V, as depicted in Fig. 2, for the most commonly used port models. The mathematical expression for the impressed field is then

$$\boldsymbol{E}^{\text{inc}}(\boldsymbol{r}) = V_m \hat{\boldsymbol{p}}_m \delta(p - p_m) \tag{2}$$

where V_m is the voltage applied at the mth port, $\hat{\boldsymbol{p}}_m$ is a unit vector collinear with the impressed field, and p_m is the location of the δ-gap in the local coordinate system attached to the port. In order to solve (1) numerically, the conducting surfaces are discretized as shown in Fig. 1 and the MoM is then utilized using specific sets of basis and testing functions. The standard choice here is the rooftop basis functions on the rectangular [13] or triangular [22] support and the rooftop or razor-blade testing functions. A typical MoM discretization in the vicinity of the port [14] is demonstrated in Fig. 2. The MoM implementation results in the impedance matrix equation [11]

$$\begin{bmatrix} \mathbf{Z}^{cc} & \mathbf{Z}^{cp} \\ \mathbf{Z}^{pc} & \mathbf{Z}^{pp} \end{bmatrix} \begin{bmatrix} \mathbf{I}^c \\ \mathbf{I}^p \end{bmatrix} = \begin{bmatrix} \mathbf{0} \\ \mathbf{V}^p \end{bmatrix} \tag{3}$$

where the superscript c denotes all the quantities associated with the elements in the circuit discretization excluding the ports, while the superscript p denotes the quantities pertinent to the ports. The vectors $\mathbf{I}^c$ and $\mathbf{I}^p$ store the unknown amplitudes of the rooftop basis functions. $\mathbf{V}^p$ is the vector of voltages applied at the MoM subsections of the ports. According to well-known network definitions, the multiport admittance matrix $\mathbf{I}^p = \mathbf{Y}^p \cdot \mathbf{V}^p$ can be obtained from the inverse of the impedance matrix $\mathbf{Z}$ in (3) as follows:

$$\begin{bmatrix} \mathbf{Y}^{cc} & \mathbf{Y}^{cp} \\ \mathbf{Y}^{pc} & \mathbf{Y}^{pp} \end{bmatrix} \begin{bmatrix} \mathbf{0} \\ \mathbf{V}_p \end{bmatrix} = \begin{bmatrix} \mathbf{I}^c \\ \mathbf{I}^p \end{bmatrix} \tag{4}$$

where $\mathbf{Y}^p = \mathbf{Y}^{pp}$ is the desired $(M \times M)$ admittance matrix of the M-port DUT.

The different types of most commonly used ports are depicted in Fig. 2. Each type of ports has advantages and disadvantages. For example, the ungrounded-internal port, shown in Fig. 2(b), is the simplest excitation mechanism for implementation in the context of MoM modeling since it is confined to the planar topology of the circuit. However, it can serve as an efficient

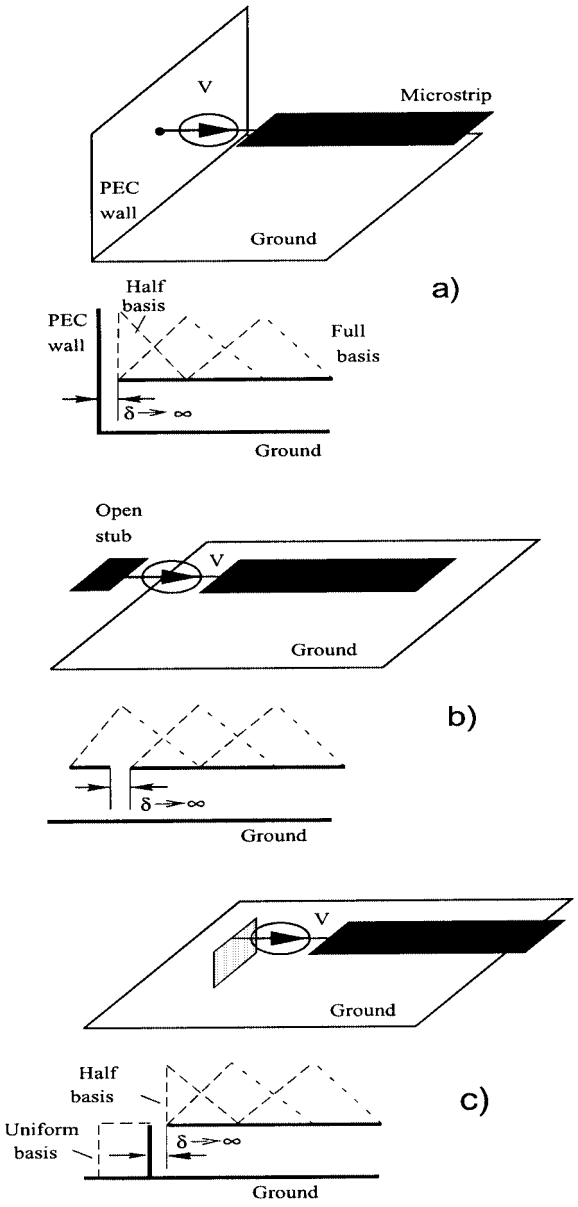

Fig. 2. Commonly used excitation mechanisms and MoM discretization in the vicinity of the exterior ports. (a) PEC wall backed up δ-gap generator. (b) Internal-ungrounded port (open stub differential port). (c) Via-port.

launcher of the TEM modes only if the operating frequency is sufficiently large so that the return path is provided through the ground by means of the displacement current. At lower frequencies, the port, being described by a capacitor in series with the voltage source, substantially impedes the current flow into the transmission line. Alternatively, the PEC wall-backed port [see Fig. 2(a)] provides an excellent excitation at any frequency; however, its numerical implementation may be more demanding since the Green's function in (1) has to accommodate for the presence of the PEC walls. In addition to that, for unbounded planar circuits, this type of port distorts the open environment around the circuit [2], unless the wall is only locally attached [5] to the ports. Therefore, unless the PEC walls are part of the DUT, their impact on the response must be eliminated in order to simulate correctly the unbounded

environment. The port mounted on a via [see Fig. 2(c)] can serve as an effective launcher of the TEM modes at any frequency and results in no distortions into the simulation of the unbounded structures. It was demonstrated in [14] that the via-port does not require deembedding when it is used to feed a relatively (electrically) large circuit such as microstrip antennas or filters, with characteristic lengths in the order of a few wavelengths or larger. For such structures, the error brought into analysis due to the parasitic effects of the higher order fields can hardly exceed the prescribed accuracy of simulation. The disadvantages of the via-ports are that they are relatively hard to implement in the MoM utilizing the multilayered media Green's function, and they are also known to be a very efficient generators of the parasitic surface waves in the substrate due to the presence of the vertical currents, which are not mitigated by the mirrored images with respect to the ground plane. The impact of the parasitic effects of the surface waves of the quality of the deembedding procedures is discussed in conjunction with the numerical studies presented in Section V.

III. Vector SOC

The SOC technique is a numerical analog of the well-established experimental transmission-thru-reflection (TRL) methodology [23]. With the definition of reference planes at the multiport interfaces of the system, as shown in Fig. 1, the entire circuit is partitioned into the error blocks, represented by the feed networks bringing signal to the reference planes and the DUT, for which network parameters, e.g., in terms of the scattering-parameter matrix for the fundamental propagating modes, are to be numerically measured. Hence, a general circuit with N groups of ports can be represented as an equivalent cascade of the error boxes and the DUT, as depicted in Fig. 3(a). The admittance parameters $\mathbf{Y}^{\Sigma}$ of the entire circuit, including the parasitic port discontinuities, can be numerically found using the MoM as prescribed by (1)–(4). In order to determine the network parameters of the multiport error boxes and, consequently, effect their removal, a "vector" version of the SOC (i.e., VSOC) methodology is required.

The VSOC computes the $\mathbf{ABCD}$ matrices of the error boxes through a set of numerical measurements simulating the idealized shorted and open termination at the reference planes. To elaborate, let us consider one of the error boxes assuming that it has P exterior ports and P ports at the corresponding reference plane. Its $(2P\times 2P)$ $\mathbf{ABCD}$-matrix [see Fig. 3(b)] relates vectors of input currents and voltages $\mathbf{I}, \mathbf{V}$ of length P to vectors of currents and voltages $\mathbf{I}', \mathbf{V}'$ defined at the reference plane and having the same length P as follows:

$$\begin{bmatrix} \mathbf{a} & \mathbf{b} \\ \mathbf{c} & \mathbf{d} \end{bmatrix} \begin{bmatrix} \mathbf{V}' \\ -\mathbf{I}' \end{bmatrix} = \begin{bmatrix} \mathbf{V} \\ \mathbf{I} \end{bmatrix}. \tag{5}$$

It is important to mention here that, for the input voltage $\mathbf{V}$, it is irrelevant whether it is defined with respect to the local ground, represented by the open stub of the internal-ungrounded port [see Fig. 2(b)] or to the ground plane, as it is featured in the wall-backed ports or via-ports [see Fig. 2(a) and (c)]. Furthermore, the voltage $\mathbf{V}'$ at the reference plane must be considered in the transmission-line sense according to the commonly used convention when working with practical planar circuits. This implies that, for the case where $\mathbf{V}' = \mathbf{0}$ [see Fig. 4(a)], the perfect short-circuit termination takes place at the reference plane for every quasi-TEM eigenmode of the MTL. Dually, the input currents $\mathbf{I}$ can be defined with much flexibility. They can either be defined as the currents in the δ-gaps or they can be measured at a plane several elements away from the gaps where the electric field $\boldsymbol{E}^{\text{inc}}$ is applied. The output currents $\mathbf{I}'$, however, are to be defined in the transmission-line sense, assuming that when $\mathbf{I}' = \mathbf{0}$ [see Fig. 4(b)], the perfect open-circuit termination is provided for all P eigenmodes in the P-conductor MTL.

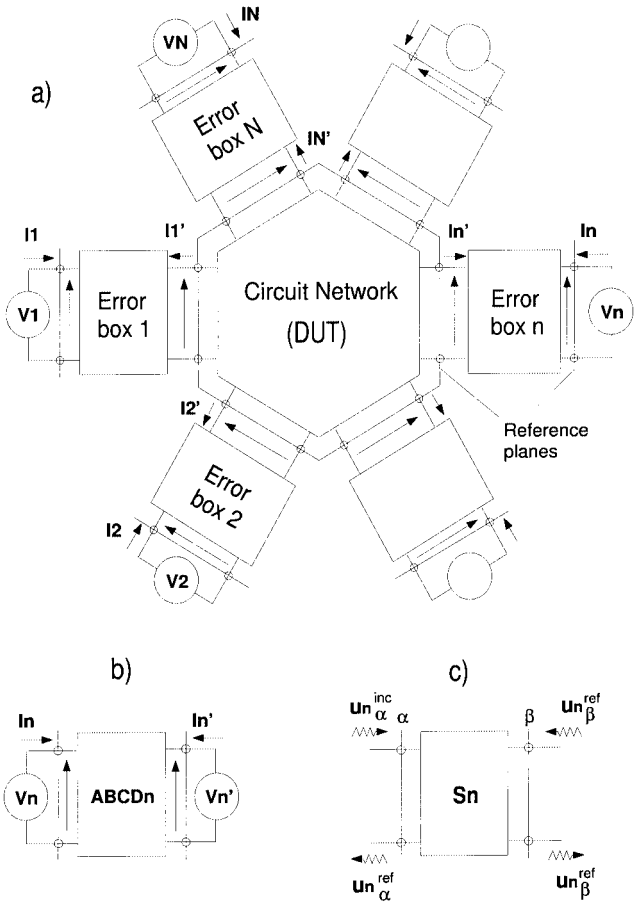

Fig. 3. Equivalent-circuit representation of the multiport device. (a) Cascade of the error boxes and DUT. (b) $\mathbf{ABCD}$-matrix description of the nth error box. (c) $\mathbf{S}$-matrix description of the nth error box.

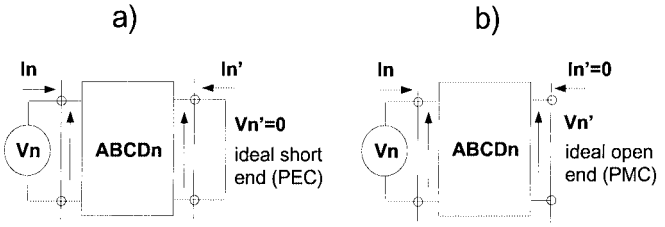

Fig. 4. Circuits for the calculation of the transmission parameters of the error box. (a) Equivalent circuit of the error box with the perfect short-circuit termination. (b) Equivalent circuit of the error box with the perfect open-circuit termination.

Following the aforementioned definitions in order to compute the $(P \times P)$ sub-matrices $\mathbf{a}, \mathbf{b}, \mathbf{c}$ and $\mathbf{d}$, the perfect short- and open-circuit termination at the reference plane for the P-conductor MTL is to be simulated. For this purpose, the layout of the error box is mirrored with respect to the reference plane, as depicted in Fig. 5. The perfect short-circuit termination is achieved when a symmetric excitation is applied, with electric fields of the same orientation impressed at the δ-gaps placed at the input ports and their mirror counterparts, as shown in Fig. 5(b). The symmetric excitation is equivalent to the excitation of the original error box terminated by a PEC wall. This excitation forces the voltage $\mathbf{V}'$ to vanish at the reference plane and, consequently, from (5), the relations

$$-\mathbf{b} \cdot \mathbf{IS}' = \mathbf{VS} \quad -\mathbf{d} \cdot \mathbf{IS}' = \mathbf{IS} \tag{6}$$

hold true. The notation "$\mathbf{S}$" is added to the quantities in order to indicate that the relevant currents and voltages are the ones for the short-circuited case. Applying P linearly independent symmetric excitations at the ports of the mirrored error box [see Fig. 5(b)] and solving the MoM impedance matrix equation (3) with the corresponding P right-hand sides, the following matrix relations are obtained:

$$-\begin{bmatrix} b_{11} & \cdots & b_{1P} \\ \vdots & \ddots & \vdots \\ b_{P1} & \cdots & b_{PP} \end{bmatrix} \cdot \begin{bmatrix} IS'_{11} & \cdots & IS'_{1P} \\ \vdots & \ddots & \vdots \\ IS'_{P1} & \cdots & IS'_{PP} \end{bmatrix} = \begin{bmatrix} VS_1 & \cdots & 0 \\ \vdots & \ddots & \vdots \\ 0 & \cdots & VS_P \end{bmatrix} \tag{7}$$

and

$$-\begin{bmatrix} d_{11} & \cdots & d_{1P} \\ \vdots & \ddots & \vdots \\ d_{P1} & \cdots & d_{PP} \end{bmatrix} \cdot \begin{bmatrix} IS'_{11} & \cdots & IS'_{1P} \\ \vdots & \ddots & \vdots \\ IS'_{P1} & \cdots & IS'_{PP} \end{bmatrix} = \begin{bmatrix} IS_{11} & \cdots & IS_{1P} \\ \vdots & \ddots & \vdots \\ IS_{P1} & \cdots & IS_{PP} \end{bmatrix}. \tag{8}$$

In (7) and (8), IS'_{ij} is the current on the ith line at the reference plane of the symmetrized error box computed by the MoM under the symmetric jth excitation, i.e., $\mathbf{VS}^T = [0 \cdots VS_j \cdots 0]$. Inversion of the matrix $\mathbf{IS}'$ and the choice $VS_j = 1$ V yields the following expressions for the sub-matrices $\mathbf{b}$ and $\mathbf{d}$:

$$\mathbf{b} = -\mathbf{IS}'^{-1} \quad \mathbf{d} = -\mathbf{IS} \cdot \mathbf{IS}'^{-1}. \tag{9}$$

Similarly, an antisymmetric excitation of the symmetrized error box is realized under condition that, in the IE (1), the electric field $\boldsymbol{E}^{\text{inc}}$ of opposite orientations [see Fig. 5(c)] is impressed at the input ports of the feed network and their mirror images. Thus, the perfect open-circuit termination of the original error box by the perfect magnetic conductor (PMC) wall

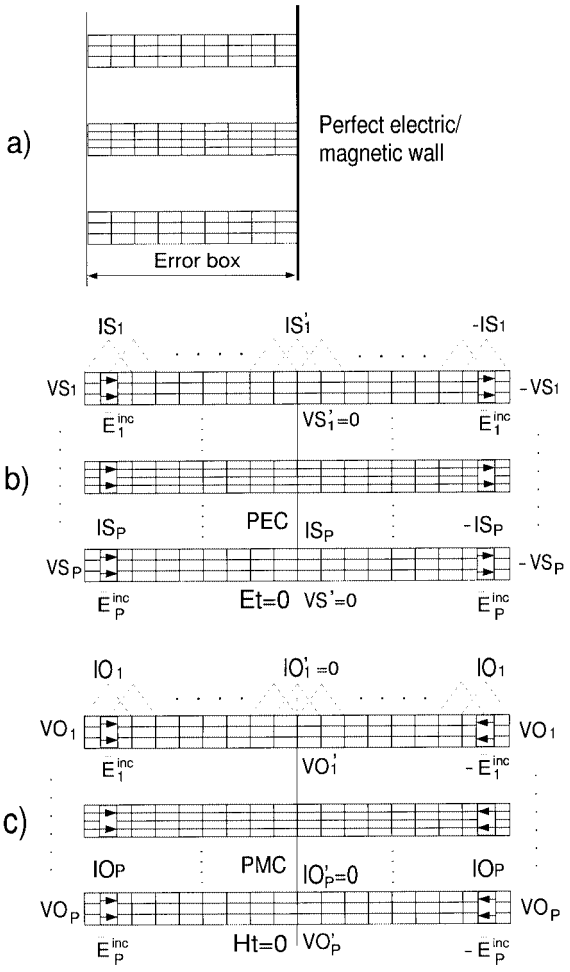

Fig. 5. Physical models of the short- and open-circuited error box. (a) Ideal short-/open-circuited error box. (b) Mirrored model of the short-circuited error box. (c) Mirrored model of the open-circuited error box.

is numerically simulated at the reference plane of the feed network. This yields $\mathbf{IO}' = \mathbf{0}$, where the character "$\mathbf{O}$" is used to indicate the currents and voltages for the case of open-circuit termination. Thus, from the definition of the transmission matrix (5), the vector of voltages $\mathbf{VO}'$ at the ends of the MTL conductors terminated at the PMC wall is related to the vectors of voltages $\mathbf{VO}$ and currents $\mathbf{IO}$ at the input ports of the error box

$$\mathbf{a} \cdot \mathbf{VO}' = \mathbf{VO} \quad \mathbf{c} \cdot \mathbf{VO}' = \mathbf{IO}. \tag{10}$$

The complete definition of the matrices $\mathbf{a}$ and $\mathbf{c}$ demands that P linearly independent excitations are employed and currents $\mathbf{IO}$ and voltages $\mathbf{VO}, \mathbf{VO}'$ are calculated, yielding the matrix form of the relations (10) as follows:

$$\begin{bmatrix} a_{11} & \cdots & a_{1P} \\ \vdots & \ddots & \vdots \\ a_{P1} & \cdots & a_{PP} \end{bmatrix} \cdot \begin{bmatrix} VO'_{11} & \cdots & VO'_{1P} \\ \vdots & \ddots & \vdots \\ VO'_{P1} & \cdots & VO'_{PP} \end{bmatrix} = \begin{bmatrix} VO_1 & \cdots & 0 \\ \vdots & \ddots & \vdots \\ 0 & \cdots & VO_P \end{bmatrix} \tag{11}$$

and

$$\begin{bmatrix} c_{11} & \cdots & c_{1P} \\ \vdots & \ddots & \vdots \\ c_{P1} & \cdots & c_{PP} \end{bmatrix} \cdot \begin{bmatrix} VO'_{11} & \cdots & VO'_{1P} \\ \vdots & \ddots & \vdots \\ VO'_{P1} & \cdots & VO'_{PP} \end{bmatrix} = \begin{bmatrix} IO_{11} & \cdots & IO_{1P} \\ \vdots & \ddots & \vdots \\ IO_{P1} & \cdots & IO_{PP} \end{bmatrix}. \quad (12)$$

IO_{ij} is the current at the ith input port of the error box when the jth antisymmetric excitation $\mathbf{VO}^T = [0 \cdots VO_j \cdots 0]$ is enforced at the jth conductor of the mirrored error box [see Fig. 5(c)]. VO'_{ij} is the voltage at the PMC wall-terminated end of the ith conductor under the jth antisymmetric excitation. In matrix notation, (11) and (12) may be recast as follows:

$$\mathbf{a} = \mathbf{VO}'^{-1} \quad \mathbf{c} = \mathbf{IO} \cdot \mathbf{VO}'^{-1}. \quad (13)$$

However, (13) cannot be directly utilized for the calculation of matrices $\mathbf{a}$ and $\mathbf{c}$. The reason is that, within the framework of the MoM solution for the mirrored feed network, the unique extraction of the voltages $\mathbf{VO}'$ at the PMC termination of the MTL cannot be done reliably at all frequencies. To circumvent this difficulty, the relationship

$$\mathbf{a} \cdot \mathbf{d} - \mathbf{c} \cdot \mathbf{b} = \mathbf{I} \quad (14)$$

which is valid for all reciprocal multiports, is employed. After some algebraic manipulations involving (9), (13), and (14), the matrix of the voltage $\mathbf{VO}'$ can be eliminated, leading to the desired matrix expressions for the blocks $\mathbf{a}$ and $\mathbf{c}$ in terms of the short-circuit case currents $\mathbf{IS}$ and $\mathbf{IS}'$ at the input ports and the reference plane, respectively, as well as the open-circuit case currents $\mathbf{IO}$ at the input ports

$$\mathbf{a} = \mathbf{IS}' \cdot (\mathbf{IO} - \mathbf{IS})^{-1} \quad \mathbf{c} = \mathbf{IO} \cdot \mathbf{IS}' \cdot (\mathbf{IO} - \mathbf{IS})^{-1}. \quad (15)$$

Hence, the $\mathbf{ABCD}$-matrix of each error box is expressed in terms of the numerically calculated currents from the MoM analysis of the mirrored feed networks under symmetric and antisymmetric excitations

$$\begin{bmatrix} \mathbf{a} & \mathbf{b} \\ \mathbf{c} & \mathbf{d} \end{bmatrix} = \begin{bmatrix} \mathbf{IS}' \cdot (\mathbf{IO} - \mathbf{IS})^{-1} & -\mathbf{IS}'^{-1} \\ \mathbf{IO} \cdot \mathbf{IS}' \cdot (\mathbf{IO} - \mathbf{IS})^{-1} & -\mathbf{IS} \cdot \mathbf{IS}'^{-1} \end{bmatrix}. \quad (16)$$

The sub-matrices $\mathbf{a}, \mathbf{b}, \mathbf{c}$ and $\mathbf{d}$ for the multiport error boxes presented in (16) have the same algebraic structure as the scalar elements a, b, c, and d derived in [13] for the two-port circuits. Clearly, they constitute the extension of the latter to the multiport case.

IV. Deembedding Through Cascaded S-Matrices

The transmission matrices $\mathbf{ABCD}_n$ of the error boxes obtained through the VSOC and the admittance parameters $\mathbf{Y}^{\mathbf{\Sigma}}$ of the entire circuit can be used to remove the port discontinuities. This removal can be accomplished through the treatment of the multiport device (Fig. 3) in terms of the cascaded connection of the $\mathbf{S}$-matrices, as shown in Fig. 6. For this purpose,

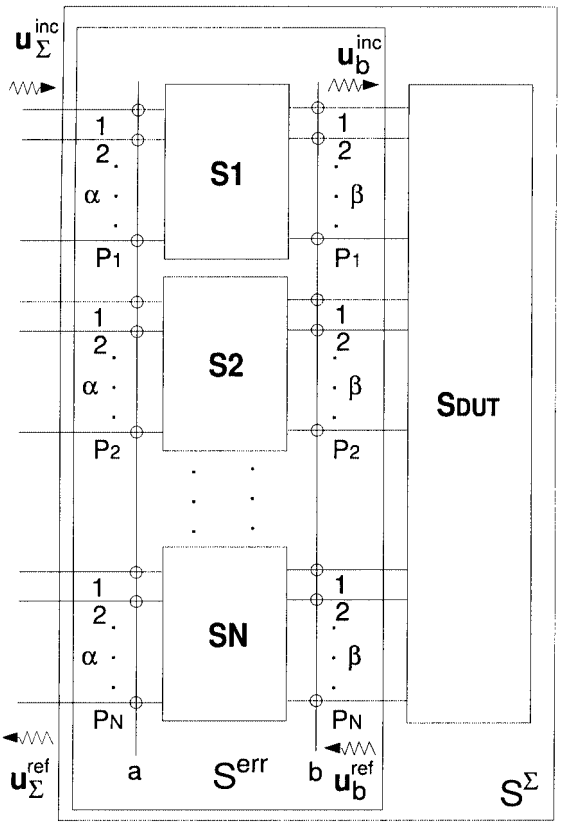

Fig. 6. Cascaded $\mathbf{S}$-matrix representation of the error boxes and the DUT in the multiport system.

it is assumed that the device has a total of $M = \sum_{n=1}^{N} P_n$ exterior ports, where N is the number of port groups and P_n is the number of ports in the nth group. With the choice of some arbitrary reference impedance Z_0, the $(M \times M)$ admittance matrix $\mathbf{Y}^{\mathbf{\Sigma}}$ of the entire circuit can be converted to the $\mathbf{S}^{\mathbf{\Sigma}}$-matrix relating the normalized vector voltage amplitudes $\mathbf{u}_{\mathbf{\Sigma}}^{\mathbf{inc}}, \mathbf{u}_{\mathbf{\Sigma}}^{\mathbf{ref}}$ of the incident and reflected waves at the input ports

$$\mathbf{S}^{\mathbf{\Sigma}} = \left(\mathbf{I} + \mathbf{y}^{\mathbf{\Sigma}}\right) \cdot \left(\mathbf{I} + \mathbf{y}^{\mathbf{\Sigma}}\right)^{-\mathbf{1}}. \quad (17)$$

In (17), $\mathbf{y}^{\mathbf{\Sigma}} = \mathbf{Y}^{\mathbf{\Sigma}} \cdot Z_0$ is the normalized admittance matrix of the circuit including the feed networks. The matrix $\mathbf{S}^{\mathbf{\Sigma}}$ is composed of N^2 sub-matrices $\mathbf{S}_{nm}^{\mathbf{\Sigma}}$, each of dimension $(P_m \times P_n)$, and expressed as

$$(\mathbf{v}_m - \mathbf{i}_m) = \mathbf{S}_{mn}^{\mathbf{\Sigma}} \cdot (\mathbf{v}_n + \mathbf{i}_n).$$

The vectors of normalized currents $\mathbf{i}_n$ and voltages $\mathbf{v}_n$ at the P_n ports of the nth-port group are related to the nonnormalized currents and voltages in terms of which the $\mathbf{Y}^{\mathbf{\Sigma}}$-matrix is defined as

$$\mathbf{i}_n = \left(\mathbf{u}_n^{\mathbf{inc}} - \mathbf{u}_n^{\mathbf{ref}}\right) = \mathbf{I}_n \sqrt{Z_0}$$
$$\mathbf{v}_n = \left(\mathbf{u}_n^{\mathbf{inc}} + \mathbf{u}_n^{\mathbf{ref}}\right) = \mathbf{V}_n / \sqrt{Z_0}.$$

In order to obtain scattering parameters of the nth $2P_n$-port feed network, where $n = 1, \ldots, N$, its $(2P_n \times 2P_n)$ transmis-

sion matrix $\mathbf{ABCD}_n$, described by (16), is converted first to the $\mathbf{Y}_n$-matrix

$$\begin{bmatrix} \mathbf{Y}_n^{\alpha\alpha} & \mathbf{Y}_n^{\alpha\beta} \\ \mathbf{Y}_n^{\beta\alpha} & \mathbf{Y}_n^{\beta\beta} \end{bmatrix} = \begin{bmatrix} \mathbf{d}_n \cdot (\mathbf{b}_n)^{-1} & \mathbf{c}_n - \mathbf{d}_n \cdot (\mathbf{b}_n)^{-1} \cdot \mathbf{a}_n \\ -(\mathbf{b}_n)^{-1} & (\mathbf{b}_n)^{-1} \cdot \mathbf{a}_n \end{bmatrix}. \tag{18}$$

Subsequently, using the same reference impedance Z_0, the scattering matrix $\mathbf{S}_n$ of the nth error box [see Fig. 4(b)]

$$\mathbf{S}_n = \begin{bmatrix} \mathbf{S}_n^{\alpha\alpha} & \mathbf{S}_n^{\alpha\beta} \\ \mathbf{S}_n^{\beta\alpha} & \mathbf{S}_n^{\beta\beta} \end{bmatrix} \tag{19}$$

can be obtained using an expression similar to (17).

Once the $\mathbf{S}$-parameters of the individual error boxes have been calculated, they are organized into the global scattering matrix of the error boxes $\mathbf{S}^{\mathrm{err}}$. For this purpose, N groups of the input ports of the entire system are unified into a single group of ports denoted by character a, while the corresponding N groups of reference plane ports of the DUT are unified into group b, as depicted in Fig. 6. Thus, the global scattering matrix of the feed networks is formulated as follows:

$$\mathbf{S}_{\mathrm{err}} = \begin{bmatrix} \mathbf{S}_{\mathrm{err}}^{aa} & \mathbf{S}_{\mathrm{err}}^{ab} \\ \mathbf{S}_{\mathrm{err}}^{ba} & \mathbf{S}_{\mathrm{err}}^{bb} \end{bmatrix} \tag{20}$$

where

$$\mathbf{S}_{\mathrm{err}}^{ij} = \begin{bmatrix} \mathbf{S}_1^{ij} & \mathbf{0} & \cdots & \mathbf{0} \\ \mathbf{0} & \mathbf{S}_2^{ij} & \cdots & \mathbf{0} \\ \vdots & \vdots & \ddots & \vdots \\ \mathbf{0} & \mathbf{0} & \cdots & \mathbf{S}_N^{ij} \end{bmatrix}. \tag{21}$$

Superscripts i and j in (21) denote either the group of ports a or the group of ports b. The zero sub-matrices in $\mathbf{S}_{\mathrm{err}}^{ij}$ indicate that the network parameters of the error boxes are treated individually, and mutual coupling between them is assumed negligible and not taken into consideration. This assumption is made in all the deembedding techniques known today. The impact of this assumption on the accuracy of the deembedding process depends on various factors, several of which are discussed in Section V.

In order to obtain the desired $\mathbf{S}$-parameter matrix of the DUT from the sub-matrices for $\mathbf{S}_{\mathrm{err}}^{ij}$ and the scattering matrix of the entire system $\mathbf{S}^{\mathbf{\Sigma}}$, the relationship between the vector amplitudes of the normalized voltage waves is established first as follows:

$$\begin{aligned} \mathbf{u}_{\mathbf{\Sigma}}^{\mathbf{ref}} &= \mathbf{S}_{\mathbf{\Sigma}} \cdot \mathbf{u}_{\mathbf{\Sigma}}^{\mathbf{inc}} \\ \mathbf{u}_{\mathbf{\Sigma}}^{\mathbf{ref}} &= \mathbf{S}_{\mathbf{err}}^{aa} \cdot \mathbf{u}_{\mathbf{\Sigma}}^{\mathbf{inc}} + \mathbf{S}_{\mathbf{err}}^{ab} \cdot \mathbf{u}_b^{\mathbf{ref}} \\ \mathbf{u}_b^{\mathbf{ref}} &= \mathbf{S}^{\mathbf{DUT}} \cdot \mathbf{u}_b^{\mathbf{inc}} \\ \mathbf{u}_b^{\mathbf{inc}} &= \mathbf{S}_{\mathrm{err}}^{ba} \cdot \mathbf{u}_{\mathbf{\Sigma}}^{\mathbf{inc}} + \mathbf{S}_{\mathbf{err}}^{bb} \cdot \mathbf{u}_b^{\mathbf{ref}}. \end{aligned} \tag{22, 23}$$

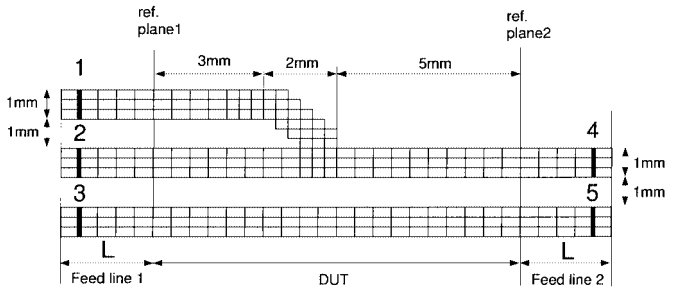

Fig. 7. Geometry and MoM discretization of the transition from three to two coupled transmission lines. The circuit is printed on a grounded lossless dielectric substrate ($\epsilon_r = 3$, thickness $d = 0.7$ mm).

From (22) and (23), the desired $(M \times M)$ scattering matrix of the DUT can be derived through the elimination of the quantities $\mathbf{u}_{\mathbf{\Sigma}}^{\mathbf{ref}}$ and $\mathbf{u}_{\mathbf{\Sigma}}^{\mathbf{inc}}$. The final result is

$$\mathbf{S}^{\mathbf{DUT}} = \left(\mathbf{S}_{\mathrm{err}}^{bb} + \mathbf{S}_{\mathrm{err}}^{ba} \cdot \left(\mathbf{S}^{\mathbf{\Sigma}} - \mathbf{S}_{\mathrm{err}}^{aa} \right)^{-1} \cdot \mathbf{S}_{\mathrm{err}}^{ab} \right)^{-1}. \tag{24}$$

V. Numerical Results and Discussion

In order to validate the proposed VSOC methodology, its application to the deembedding of various multiport planar circuits has been considered. The method has been found to exhibit both the robustness and versatility needed for the accurate broad-band deembedding of most multiport circuits encountered commonly in practical microwave—and millimeter-wave integrated circuits and high-speed digital interconnect structures. For the specific examples presented in this section, the internal ungrounded ports [see Fig. 2(b)] with the local ground references were used to drive the circuits. The width of the MTL conductors was taken to be 1 mm and at least three MoM discretization cells were introduced across the conductor width.

A. Transition From Three to Two Coupled Lines

The first considered structure is the transition from three to two coupled transmission lines with geometry and MoM discretization depicted in Fig. 7 for the case of 2.5 mm-long feed lines. The circuit is printed on a PEC-backed lossless dielectric layer of thickness 0.7 mm and relative permittivity $\epsilon_r = 3$. Perfect conductors of zero thickness are assumed. The internal ungrounded ports were introduced a half MoM subsection away from the ends of the lines where the open stubs provided the local ground for each port, as shown in Fig. 2(b). The location of the exterior ports is marked in Fig. 7 by the thick lines at the ends of the MTLs. Deembedding of the error boxes was performed for three different lengths of the feed networks $L = 2.5$ mm, 3.5 mm, and 5 mm. The deembedded scattering parameters of the device for the cases when the excitation is applied at the first and the second ports are depicted in Figs. 8 and 9, respectively. The S-parameters obtained as a result of the deembedding of the different feed networks are in very good agreement over a wide range of frequencies, indicating that the proposed VSOC methodology is effective and accurate. To provide an independent reference, the same circuit was simulated using Sonnet

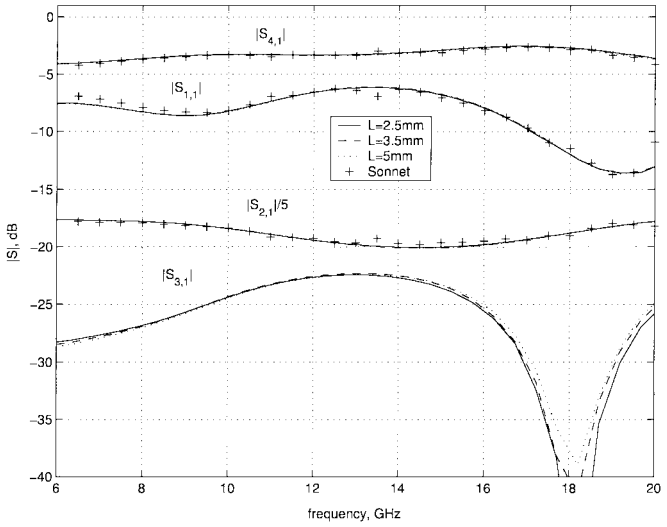

Fig. 8. Deembedded $S_{n,1}$-parameters for different lengths L of the error boxes.

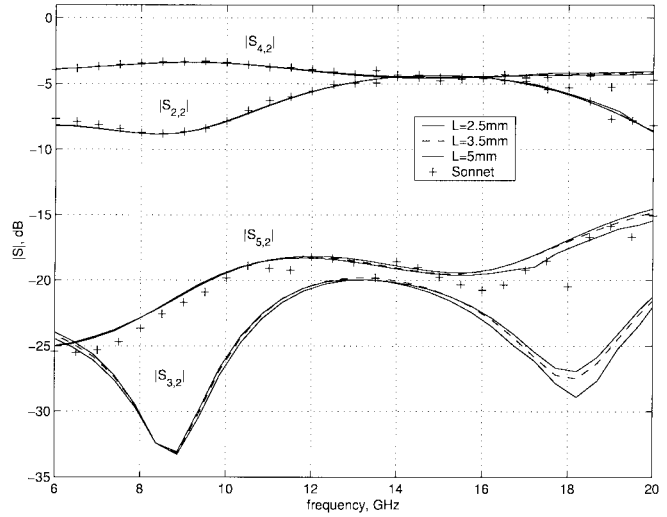

Fig. 9. Deembedded $S_{n,2}$-parameters for different lengths L of the error boxes.

high-frequency EM software [2]. The "reference" S-parameters obtained from Sonnet are also shown in Figs. 8 and 9. The VSOC results are in very good agreement with the Sonnet results for this structure. It is mentioned that, through several numerical experiments, it was found that the accuracy obtained from the VSOC deembedding was superior to that of Sonnet for the case of weakly coupled ports. This observation was consistent with the comparisons made in [17].

It can be seen that disagreement between the S-parameters for different lengths L becomes more pronounced for the weakly coupled ports (e.g., $S_{3,1}$) at higher frequencies. This behavior was observed for all structures considered. It is attributed to the fact that, at higher frequencies, EM coupling between the feed lines of these ports through mechanisms unaccounted for in (21) increases in its relative value with respect to the natural coupling between these ports in the DUT. The primary contribution to this coupling is provided by the surface wave excited

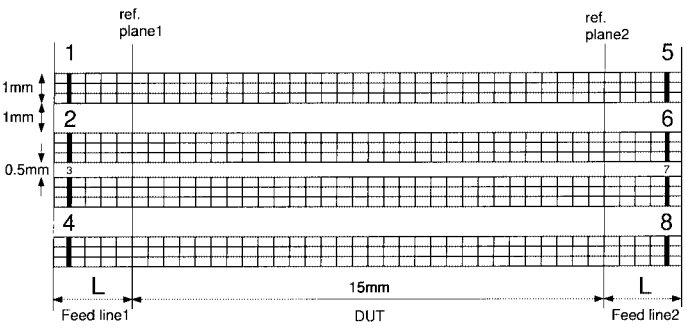

Fig. 10. Geometry and MoM discretization of a coupled uniform four-conductor microstrip system. The circuit is printed on a grounded or ungrounded substrate ($\epsilon_r = 3$, thickness $d = 0.7$ mm).

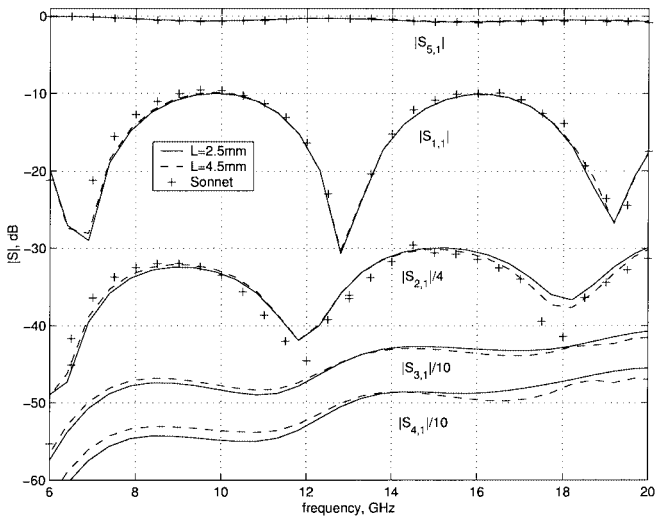

Fig. 11. Deembedded $\mathbf{S}$-parameters for the four-conductor microstrip line on the grounded substrate for different lengths L of the error boxes.

in the dielectric substrate. As frequency increases, both the electric thickness of the dielectric substrate and the electric length of the feed lines increase. This intensifies the surface-wave excitation by the driven feed lines and makes the victim feed lines more susceptible to their reception. As a result, the unaccounted coupling increases. In this sense, the feed networks act as two antennas located in the close proximity of each other and their coupling depends on the mutual location, electric length, and propagation channel between the antennas.

B. Four Coupled Lines Printed on Grounded and Ungrounded Substrates

The second numerical study considers a 15-mm stretch of four uniform coupled transmission lines. The geometry of the circuit and its MoM discretization are shown in Fig. 10 for the case of the 2.5-mm-long error boxes. First, the circuit was considered on top of a PEC-backed 0.7-mm-thick nonmagnetic dielectric substrate of relative permittivity $\epsilon_r = 3$. To ensure the consistency of the numerical computations, the feed lines of two different lengths $L = 2.5$ mm and $L = 4.5$ mm were used to deliver the signal to the circuit and subsequently deembedded using the VSOC technique. The computed S-parameters are depicted in Fig. 11. Shown in the same figure are scattering

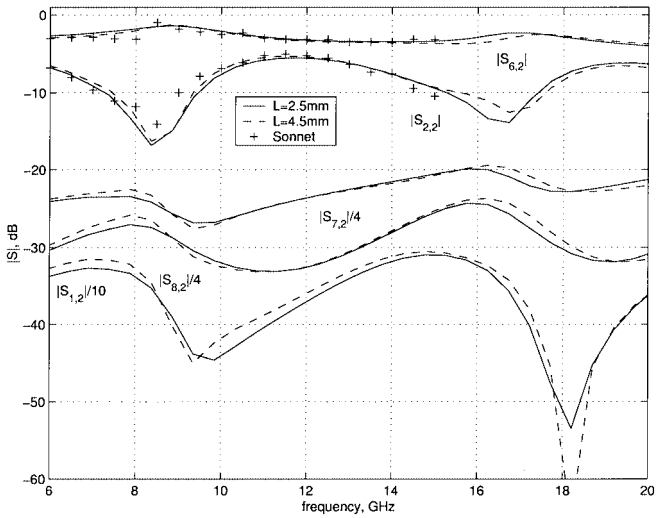

Fig. 12. Deembedded **S**-parameters for the four-conductor microstrip line on the ungrounded substrate for different lengths L of the error boxes.

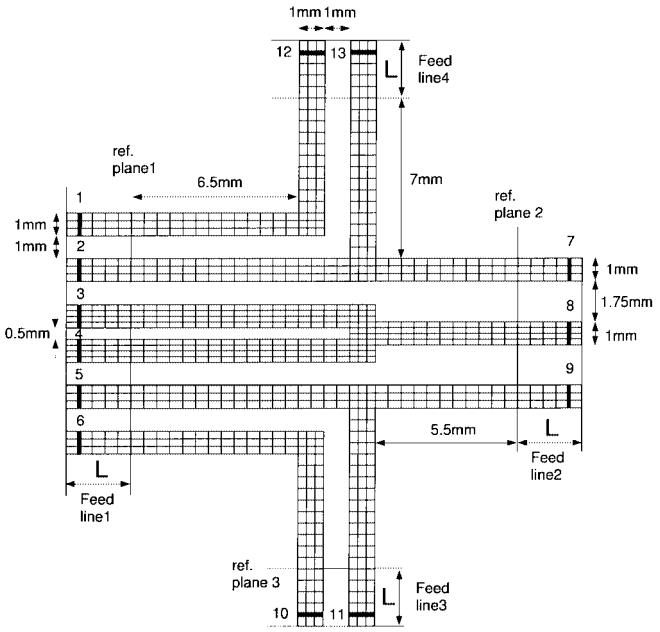

Fig. 13. Geometry and MoM discretization of a 13-port circuit.

parameters of the circuit generated with the Sonnet EM simulator. Good agreement is observed over the frequency range of simulation.

For frequencies above 20 GHz, the leakage of power into the surface waves of the substrate becomes relatively high. For this particular structure at 30 GHz, the parasitic coupling of the error boxes by means of the surface wave reached the level at which the deembedding accuracy reduced to 90% for $S_{1,1}$ and became even lower for the weakly coupled ports of the system for which the transmission coefficients are small. It is important to mention here that, for those cases for which surface-wave coupling becomes significant, the MoM schemes using the nonlocal PEC wall backing up the ports [see Fig. 2(a)] completely fail in simulating the unbounded environment around the device because of the surface wave bouncing back from the walls and strongly interfering with the DUT.

The removal of the ground plane backing up the dielectric substrate used for the four-conductor MTL leads to a new coupled transmission-line structure expected to show more significant surface-wave effects, as well as power loss due to radiation. The thickness and dielectric constant of the substrate were kept the same as before ($d = 0.7$ mm, $\epsilon_r = 3$). The deembedded S-parameters of the four conductor MTL on the ungrounded substrate obtained are depicted in Fig. 12 for $L = 2.5$ and 4.5 mm lengths of the error boxes. A lower accuracy of deembedding in this case compared to the results for the grounded substrate example is a result of a much stronger excitation of the surface wave in the ungrounded substrate, which introduces the coupling between the error boxes unaccounted for in the VSOC. Despite stronger surface-wave coupling, a relatively good agreement of the results is observed over a wide band of frequencies. The consistency of the VSOC deembedding procedure for the MTL on the ungrounded substrate supports the idea of local grounds introduced at the ports. From this point-of-view, any type of ports presented in Fig. 2 and other port configurations not discussed in this paper can be viewed as launchers of the quasi-TEM eigenmodes of a coupled transmission-line system, providing the "test ground" for the numerical modeling of the circuit. Subsequently, independent of the particular excitation scheme used for the numerical modeling of the circuit, its contribution to the DUT network parameters can be removed through the VSOC. This leads to the conclusion that the introduction of the PEC walls, which, according to conventional wisdom must locally or globally back the δ-gap generators at the ports, can be viewed as a redundancy, which can and should be eliminated whenever accurate simulation of a planar circuit in an unbounded environment is required. Removal of this restriction enriches the framework of MoM modeling by allowing a substantial flexibility in the choice of excitation mechanisms.

C. 13-Port Device

The layout of the 13-port device and its discretization for the case when the length L of the feed lines at each group of ports is equal to 2.5 mm is shown in Fig. 13. The assessment of the numerical overhead associated with evaluation of the feed circuit network parameters can be done from the following details of the MoM implementation. The discretization of the circuit including the 2.5-mm feed lines involved 1415 rooftop basis functions at all frequencies. The number of basis functions used to discretize the first, second, third, and forth mirrored error boxes (Fig. 5) of the length $L = 2.5$ mm were taken to be 320, 160, 94 and 94, respectively. The scattering parameters of the device printed of the 0.7-mm-thick grounded dielectric substrate of relative permittivity $\epsilon_r = 3$ were deembedded as a result of three numerical experiments involved three different lengths of the error boxes $L = 2.5$ mm, 3.5 mm, and 4.5 mm. The results of the deembedding are shown in Fig. 14. The same circuit was analyzed with the Sonnet EM software and the calculated S-parameters are plotted in this same figure.

From Fig. 14, it is apparent that high accuracy and consistency of the VSOC deembedding is achieved at all frequencies for which the parasitic coupling of the feed networks through

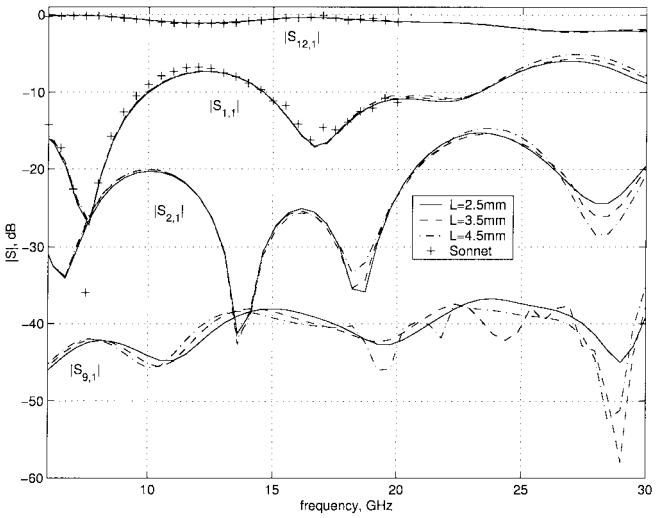

Fig. 14. Deembedded $\mathbf{S}$-parameters for the 13-port circuit for different lengths L of the error boxes. The circuit is printed on a 0.7-mm-thick grounded dielectric substrate of relative permittivity $\epsilon_r = 3$.

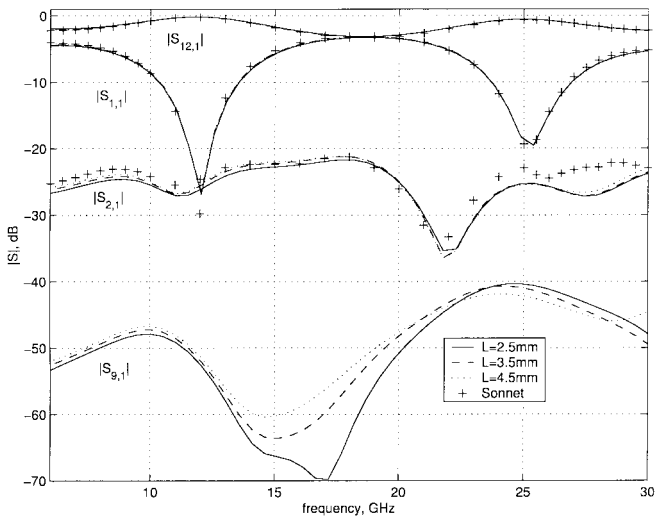

Fig. 15. Deembedded $\mathbf{S}$-parameters for different lengths L of the error boxes. The circuit is printed on a 0.7-mm-thick grounded dielectric substrate of relative permittivity $\epsilon_r = 1$.

surface waves is negligible. When the frequency is high enough for the parasitic surface-wave coupling to reach levels comparable to the quasi-TEM eigenmode-induced coupling, the weak interactions in the system cannot be accurately extracted. In Fig. 14, the curve corresponding to the coupling of the first and ninth ports $(S_{9,1})$ is a typical example of the situation when the surface-wave coupling is comparable in strength with a specific transmission coefficient in the system.

In order to demonstrate how the removal of the parasitic surface-wave interactions between the feed networks improves the accuracy of deembedding, the same 13-port device was considered in a setup that does not support the surface waves. Namely, the relative permittivity of the substrate was assumed to be that of air with the rest of the modeling parameters kept intact. The results of this numerical experiment are depicted in Fig. 15. One can see improved accuracy of the deembedding at the higher frequencies where previously the surface-wave excitation (due to presence of the dielectric substrate) had a substantial impact on the deembedded (weak) transmission coefficients.

It is important to emphasize that the unaccounted parasitic surface-wave interactions between the transmission lines in the feed networks of the system are not the only source of potential error in the VSOC. Their contribution into the error of deembedding is dominant only under condition that the overall error of the MoM implementation is kept at a level considerably below the parasitic surface-wave interactions. If this is not the case, however, the common rule applies that none of the weak interaction in the DUT can be accurately modeled unless they substantially exceed the numerical error of the MoM analysis.

Another factor that can potentially cause a large error in the deembedding process is the insufficient length L of the error boxes. In the VSOC scheme, the DUT and error boxes are assumed to be related only through the conductor currents at the reference planes. Therefore, if the ports where the electric field is impressed are not moved sufficiently far away from the reference plane, the unaccounted interference (due to higher order fields produced around the ports) with the DUT may cause a higher error in the deembedding process. However, the lengths of the feed lines should not be excessive since the longer the feed lines are, the stronger their excitation and susceptibility to surface waves at higher frequencies is. Through extensive numerical experimentations, it was found that the best accuracy of the VSOC is achieved when the length of feed lines is confined within bounds $0.2 < L/\lambda_{\text{eff}} < 0.4$, where λ_{eff} is the effective wavelength of the layered media the circuit is printed on.

VI. Conclusion

In this paper, an accurate and systematic methodology has been presented and validated for broad-band numerical deembedding of scattering parameters of multiport microwave devices. The proposed methodology, called the VSOC, was based on the idea of the earlier-proposed SOC, and constitutes its systematic extension to the case of multiport circuit topologies with arbitrary number of coupled ports. The VSOC method is compatible with the IE-based MoM modeling of planar circuits and overcomes many of the shortcomings and implementation difficulties of commonly used deembedding procedures, particularly those associated with inconsistencies between the two-dimensional quasi-TEM modeling of the coupled transmission-line feed networks and the three-dimensional full-wave circuit modeling of the DUT. Through several numerical experiments, it has been demonstrated that the VSOC methodology, taking advantage of the distributed nature of microwave circuits, offers substantial flexibility in the choice of the numerical excitation mechanisms that can be exercised for the deembedding of quasi-TEM mode-based scattering parameters of multiport planar circuits. For example, it has been shown that the use of PEC walls to back δ-gap generators used in the deembedding of unshielded planar circuits is redundant and, thus, can and should be avoided since they disturb the actual physical topography of the planar circuit and, consequently, may cause spurious perturbations to its EM response, especially at higher frequencies.

REFERENCES

[1] F. Ling and J.-M. Jin *et al.*, "Full-wave analysis of multilayer microstrip problems," in *Fast and Efficient Algorithms in Computational Electromagnetics*, W. C. Chew *et al.*, Eds. Boston, MA: Artech House, 2001, pp. 729–772.

[2] *The Sonnet User's Manual*, Sonnet Software Inc., Liverpool, NY, Apr. 1999.

[3] J. R. Mosig, "Integral equation technique," in *Numerical Techniques for Microwave and Millimeter-Wave Passive Structures*, T. Itoh, Ed. New York: Wiley, 1989, pp. 133–214.

[4] A. M. Lerer and A. G. Schuchinsky, "Full-wave analysis of three-dimensional planar structures," *IEEE Trans. Microwave Theory Tech.*, vol. 41, pp. 2002–2015, Nov. 1993.

[5] L. Zhu and K. Wu, "Characterization of unbounded multiport microstrip passive circuits using an explicit network-based method of moments," *IEEE Trans. Microwave Theory Tech.*, vol. 45, pp. 2114–2124, Dec. 1997.

[6] W. C. Chew *et al.*, "Introduction to electromagnetic analysis and computational electromagnetics," in *Fast and Efficient Algorithms in Computational Electromagnetics*, W. C. Chew *et al.*, Eds. Boston, MA: Artech House, 2001, pp. 1–26.

[7] A. C. Polycarpou, P. A. Tirkas, and C. A. Balanis, "The finite-element method for modeling circuits and interconnects for electronic packaging," *IEEE Trans. Microwave Theory Tech.*, vol. 45, pp. 1868–1874, Oct. 1997.

[8] D. M. Sheen, S. M. Ali, M. D. Abouzahra, and J. A. Kong, "Application of the three-dimensional finite-difference time-domain method to the analysis of planar microstrip circuits," *IEEE Trans. Microwave Theory Tech.*, vol. 38, pp. 849–857, July 1990.

[9] L. P. B. Katehi and N. G. Alexopoulos, "Frequency-dependent characteristics of microstrip discontinuities in millimeter-wave integrated circuits," *IEEE Trans. Microwave Theory Tech.*, vol. MTT-33, pp. 1029–1035, Oct. 1985.

[10] R. W. Jackson and D. M. Pozar, "Full-wave analysis of microstrip open-end and gap discontinuities," *IEEE Trans. Microwave Theory Tech.*, vol. MTT-33, pp. 1036–1042, Oct. 1985.

[11] G. V. Eleftheriades and R. Mosig, "On the network characterization of planar passive circuits using the method of moments," *IEEE Trans. Microwave Theory Tech.*, vol. 44, pp. 438–445, Mar. 1996.

[12] H. Y. Yang and N. G. Alexopoulos, "Basic blocks for high frequency interconnects: Theory and experiment," *IEEE Trans. Microwave Theory Tech.*, vol. 36, pp. 1258–1264, Aug. 1988.

[13] L. Zhu and K. Wu, "Unified equivalent-circuit model of planar discontinuities suitable for field theory-based CAD and optimization of M(H)MIC's," *IEEE Trans. Microwave Theory Tech.*, vol. 47, pp. 1589–1602, Sept. 1999.

[14] M. N. Abdulla and M. B. Steer, "Extraction of network parameters in the electromagnetic analysis of planar structures using the method of moments," *IEEE Trans. Microwave Theory Tech.*, vol. 49, pp. 94–103, Jan. 2001.

[15] E. K. L. Yeung, J. C. Beal, and Y. M. M. Antar, "Multilayer microstrip structure analysis with matched load simulation," *IEEE Trans. Microwave Theory Tech.*, vol. 43, pp. 143–149, Jan. 1995.

[16] K. M. Coperich, J. Morsey, V. I. Okhmatovski, A. C. Cangellaris, and A. E. Ruehli, "Systematic development of transmission-line models for interconnects with frequency-dependent losses," *IEEE Trans. Microwave Theory Tech.*, vol. 49, pp. 1677–1685, Oct. 2001.

[17] L. Zhu and K. Wu, "Comparative investigation on numerical de-embedding techniques for equivalent circuit modeling of lumped and distributed microstrip circuits," *IEEE Microwave Wireless Comp. Lett.*, vol. 12, pp. 51–53, Feb. 2002.

[18] W. C. Chew, *Waves and Fields in Inhomogeneous Media*. Piscataway, NJ: IEEE Press, 1995.

[19] K. A. Michalski and D. Zheng, "Electromagnetic scattering and radiation by surfaces of arbitrary shape in layered media, part I: Theory," *IEEE Trans. Antennas Propagat.*, vol. 38, pp. 335–344, Mar. 1990.

[20] M. I. Aksun, "A robust approach for the derivation of closed-form Green's functions," *IEEE Trans. Microwave Theory Tech.*, vol. 44, pp. 651–658, May 1996.

[21] V. I. Okhmatovski and A. C. Cangellaris, "A new technique for the derivation of closed-form electromagnetic Green's function's for unbounded planar layered media," *IEEE Trans. Antennas Propagat.*, vol. 50, pp. 1005–1016, July 2002.

[22] S. S. M. Rao, D. R. Wilton, and A. W. Glisson, "Electromagnetic scattering by surfaces of arbitrary shapes," *IEEE Trans. Antennas Propagat.*, vol. AP-30, pp. 409–418, May 1982.

[23] R. R. Pantoja, M. J. Howes, J. R. Richardson, and R. D. Pollard, "Improved calibration and measurement of the scattering parameters of microwave integrated circuits," *IEEE Trans. Microwave Theory Tech.*, vol. 37, pp. 1675–1680, Nov. 1989.

[24] W.-L. Wu, A. W. Glisson, and D. Kajfez, "A study of two numerical solution procedures for the electric field integral equation at low frequency," *Appl. Comput. Electromagn. Soc. J.*, vol. 10, no. 3, pp. 69–80, Nov. 1995.

Vladimir I. Okhmatovski (M'99) was born in Moscow, Russia, in 1974. He received the M.S. (with distinction) and Candidate of Science (Ph.D.) degrees from the Moscow Power Engineering Institute, Moscow, Russia, in 1996 and 1997, respectively.

In 1997, he joined the Radio Engineering Department, Moscow Power Engineering Institute, as an Assistant Professor. From 1998 to 1999, he was a Post-Doctoral Fellow with the Microwave Laboratory, National Technical University of Athens, Athens, Greece. In 1999, he joined the Department of Electrical and Computer Engineering, University of Illinois at Urbana-Champaign, where he is currently a Post-Doctoral Research Associate. He has authored and coauthored over 30 papers in professional journals and conference proceedings. His research interests include fast algorithms in computational electromagnetics, modeling of high-speed interconnects, geometrical and physical theories of diffraction, and conformal antennas and arrays.

Dr. Okhmatovski was the recipient of a 1995 scholarship of the Government of the Russian Federation, a 1996 Presidential Scholarship of the Russian Federation, and a 1997–2000 scholarship of the Russian Academy of Science. In 1996, he was the recipient of the Second Prize for the Best Young Scientist Report presented at the VI International Conference on Mathematical Methods in Electromagnetic Theory (MMET'96). He was also the recipient of the Outstanding Technical Paper Award at the Third Electronics Packaging Technology Conference (EPTC 2000).

Jason Morsey (S'01) received the B.S. (*cum laude*) and M.S. degrees from Clemson University, Clemson, SC, in 1998 and 2000, respectively, both in electrical engineering, and the Ph.D. degree from the University of Illinois at Urbana-Champaign in 2003.

He was a co-op student with Reliance Electric and W. R. Grace. He is currently with the IBM T. J. Watson Research Center, Yorktown Heights, NY. His research had been focused on near-field antennas. His current research interests include EM modeling of high-speed on-chip interconnects and signal integrity analysis.

Andreas C. Cangellaris (M'86–SM'96–F'00) received the M.S. and Ph.D. degrees in electrical and computer engineering from the University of California at Berkeley, in 1983 and 1985, respectively.

He is currently a Professor of electrical and computer engineering with the University of Illinois at Urbana-Champaign (UIUC). Prior to joining UIUC, he was on the faculty of the Electrical and Computer Engineering, University of Arizona, initially as an Assistant Professor (1987–1992) and then as an Associate Professor (1992–1997). Prior to that, he was a Senior Research Engineer with the Electronics Department, General Motors Research Laboratories, Warren, MI (1985–1987). His research has concerned the area of applied and computational electromagnetics with emphasis on their application to electrical modeling and simulation of RF/microwave components and systems, high-speed digital interconnects at the board, package, and chip level, as well as the modeling and simulation of EMC and electromagnetic interference (EMI). He has coauthored over 150 refereed papers and three book chapters on topics related to computational electromagnetics and interconnects and package modeling and simulation. Over the past 14 years, he has supervised the development of EM modeling methodologies and numerous computer modeling and simulation tools for high-speed/high-frequency signal integrity-driven applications, which have been transferred successfully to industry.

Prof. Cangellaris is an active member of the IEEE Microwave Theory and Techniques Society (IEEE MTT-S), the IEEE Components Packaging and Manufacturing Technology Society, the IEEE Antennas and Propagation Society (IEEE AP-S), and the IEEE Magnetics Society. He serves as member of Technical Program Committees for major conferences and symposia sponsored by these societies. He has served as associate editor for the IEEE TRANSACTIONS ON ANTENNAS AND PROPAGATION and is currently associate editor for the IEEE TRANSACTIONS ON ADVANCED PACKAGING and the IEEE Press Series on Electromagnetic Fields and Waves. He is the co-founder of the IEEE Topical Meeting on Electrical Performance of Electronic Packaging.